











RESEARCH ARTICLE | MARCH 01 2024

Multifunctional scaffolds for biomedical applications: Crafting versatile solutions with polycaprolactone enriched by graphene oxide

G. Friggeri ; I. Moretti ; F. Amato ; A. G. Marrani ; F. Sciandra ; S. G. Colombaroli ; A. Vitali ;
S. Viscuso ; A. Augello ; L. Cui ; G. Perini ; M. De Spirito  ; M. Papi  ; V. Palmieri 



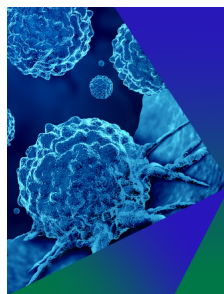
APL Bioeng. 8, 016115 (2024)

<https://doi.org/10.1063/5.0184933>



CrossMark

04 March 2024 09:31:24



Biophysics Reviews

Special Topic: Biomolecular Phase Transitions and the
Mechanochemical Control of Cells in Health & Disease

Submit Today



Multifunctional scaffolds for biomedical applications: Crafting versatile solutions with polycaprolactone enriched by graphene oxide



Cite as: APL Bioeng. 8, 016115 (2024); doi: 10.1063/5.0184933

Submitted: 27 October 2023 · Accepted: 30 January 2024 ·

Published Online: 1 March 2024



View Online



Export Citation



CrossMark

G. Friggeri,^{1,2} I. Moretti,¹ F. Amato,³ A. G. Marrani,³ F. Sciandra,⁴ S. G. Colombaroli,⁴ A. Vitali,⁴ S. Viscuso,⁴ A. Augello,^{1,2} L. Cui,¹ G. Perini,^{1,2} M. De Spirito,^{1,2,a)} M. Papi,^{1,2,5,a)} and V. Palmieri,^{1,2,5}

AFFILIATIONS

¹Dipartimento di Neuroscienze, Università Cattolica del Sacro Cuore, Largo Francesco Vito 1, 00168 Roma, Italy

²Fondazione Policlinico Universitario "A. Gemelli" IRCSS, Largo A. Gemelli 8, 00168 Roma, Italy

³Dipartimento di Chimica, Università di Roma "La Sapienza," p.le A. Moro 5, I-00185 Roma, Italy

⁴Istituto di Scienze e Tecnologie Chimiche "Giulio Natta"-SCITEC (CNR), C/O Istituto di Biochimica e Biochimica Clinica, Università Cattolica del Sacro Cuore, L.go F. Vito 1, 00168-Roma, Italy

⁵Istituto dei Sistemi Complessi, CNR, via dei Taurini 19, 00185 Roma, Italy

^{a)}Authors to whom correspondence should be addressed: marco.despirito@unicatt.it and Massimiliano.papi@unicatt.it

ABSTRACT

The pressing need for multifunctional materials in medical settings encompasses a wide array of scenarios, necessitating specific tissue functionalities. A critical challenge is the occurrence of biofouling, particularly by contamination in surgical environments, a common cause of scaffolds impairment. Beyond the imperative to avoid infections, it is also essential to integrate scaffolds with living cells to allow for tissue regeneration, mediated by cell attachment. Here, we focus on the development of a versatile material for medical applications, driven by the diverse time-definite events after scaffold implantation. We investigate the potential of incorporating graphene oxide (GO) into polycaprolactone (PCL) and create a composite for 3D printing a scaffold with time-controlled antibacterial and anti-adhesive growth properties. Indeed, the as-produced PCL-GO scaffold displays a local hydrophobic effect, which is translated into a limitation of biological entities-attachment, including a diminished adhesion of bacteriophages and a reduction of *E. coli* and *S. aureus* adhesion of ~81% and ~69%, respectively. Moreover, the ability to 3D print PCL-GO scaffolds with different heights enables control over cell distribution and attachment, a feature that can be also exploited for cellular confinement, i.e., for microfluidics or wound healing applications. With time, the surface wettability increases, and the scaffold can be populated by cells. Finally, the presence of GO allows for the use of infrared light for the sterilization of scaffolds and the disruption of any bacteria cell that might adhere to the more hydrophilic surface. Overall, our results showcase the potential of PCL-GO as a versatile material for medical applications.

© 2024 Author(s). All article content, except where otherwise noted, is licensed under a Creative Commons Attribution (CC BY) license (<http://creativecommons.org/licenses/by/4.0/>). <https://doi.org/10.1063/5.0184933>

INTRODUCTION

The requirement for multifunctional materials for medical applications is undeniable, driven by the diverse and dynamic demands of the human body.¹ Each specific application necessitates tailored materials that can seamlessly integrate into the complex physiological environment through specific surface and bulk functionalities. Achieving this level of versatility is of paramount importance for enhancing the safety, effectiveness, and longevity of medical devices, ultimately paving the way for innovative solutions that can address the intricate needs of *in vivo* applications. One such material that shows great

promise is polycaprolactone (PCL), a biodegradable polyester that has gained attention in various biomedical fields. PCL's low toxicity, biocompatibility, and 3D printability provide an attractive choice for medical products such as absorbable sutures and wound closure devices,² drug delivery systems,³ scaffolds for tissue engineering,⁴ such as bone,⁵ cartilage,⁶ and skin,⁷ catheters,⁸ and stents.^{9,10} Despite these advantageous properties, PCL alone lacks intrinsic antibacterial capabilities, which limit its ability to prevent infections such as surgical site infections (SSIs), that pose a substantial threat in surgical environments. Various factors significantly heighten the risk of SSIs, such as

preexisting infections, extended hospital stays, suboptimal surgical procedures, prolonged surgical durations, and inadequate sterilization of surgical instruments.¹¹ To address this issue, the incorporation of antibacterial materials into PCL has been explored to enhance its performance.¹²

However, biofouling, the accumulation and growth of biomacromolecules that can lead to the deterioration or impairment of implants, encompasses a wide range of lengths and time scales, making it a highly dynamic process strictly dependent on surface features.¹³ Specifically, while hydrophilicity is required to improve protein adsorption and tissue integration, hydrophobicity increases self-cleaning properties prolonging the device lifespan and reducing friction. Hydrophobic polymer surfaces can also improve long-term mechanical behavior.¹⁴ However, the intrinsic hydrophobicity of PCL leads to a lack of recognition sites attached by cells on the surface and limits cell spreading on scaffolds.

In summary, though the quick adsorption of proteins upon implantation serves as a foundation for microorganisms bacteria to settle and form biofilms, it also plays a crucial role in cell adhesion.^{13,15} Therefore, spatiotemporal control of biological adhesion on scaffolds is desirable to (i) initially inhibit SSI and (ii) favor cell adhesion and tissue repair on scaffolds at a later stage.

In terms of enhancing the properties of polymers, nanomaterials represent a recent solution. In this field, graphene, a two-dimensional (2D) carbon nanomaterial, and its derivatives with large surface area, high mechanical strength, excellent electrical conductivity, and inherent antibacterial effects have been largely studied as part of 3D printable composites.^{16,17} Graphene carbon atoms are spaced at a distance of 0.142 nm forming a hexagonal lattice with sp^2 hybridization. Each atom shares three of its outer shell electrons to form covalent σ -bonds, while the fourth electron, in a p_z orbital, participates in the formation of a π bond. Unlike the sp^2 orbitals, the linear combination of the p_z orbitals allows for a long-range delocalization of π electrons, which can move above and below the 2D graphene sheet. Such an extended delocalization of π electrons is responsible for the extraordinary electrical conductivity of graphene derivatives.^{18–23} Graphene's remarkable strength arises from its robust in-plane carbon-carbon σ -bonds. Composite materials incorporating graphene have significant advantages due to its low density (approximately 2300 kg/m³) and substantial Young's modulus (around 1 TPa).²⁴ Graphene oxide (GO) represents an oxidized variant of graphene with the presence of oxygenated functional groups. These groups yield several consequences, including the partial disruption of the extended π -network with the creation of defects, the increase in the interlayer spacing as well as the decrease in electrical conductivity. Reduced graphene oxide (rGO), on the other hand, stands as a deoxygenated iteration of GO.^{25,26} While the reduction processes do not fully recover the pristine graphene structure, the removal of oxygen groups results in an increased C/O ratio, a tunable restoration of the sp^2 structure, improved mechanical strength, expanded surface area, enhanced stability, hydrophobic characteristics, and an increase in electrical conductivity.^{27,28} Graphene, GO, and rGO possess distinctive bioactive properties due to their surface groups and consequently to their capacity of dissolving in apolar and polar solvents, respectively. At present, there is a consensus within the scientific community that properly designed graphene materials not only exhibit biocompatibility but also frequently outperform in creating an optimal microenvironment for cell growth and

differentiation. Indeed, several graphene-based materials have been used in scaffold applications for nerve, bone, muscle regeneration, and wound healing.^{29,30}

In this work, polar solvent-soluble GO, functionalized with alkylamine groups, has been used to obtain a temporally controlled bioactivity of 3D-printed PCL scaffolds. So far, the temporal control of graphene properties has been proposed in *in vitro* applications for diagnostic purpose,^{31,32} to control mechanical properties of scaffolds³³ or to control cell or drug release^{34–36} rather than modulating cell attachment and biofouling on scaffolds. Composites of graphene derivatives and PCL have also been studied; however, frequently, GO has been reduced to rGO to allow for proper mixing with PCL³⁷ since GO is poorly soluble in organic solvents compared to rGO and might result in non-uniform composites.^{38,39}

In our work, the presence of alkylamine groups is used not only to enhance the dispersibility of GO in organic solvents but also to control surface hydrophobicity during contact with biological fluids. This modified graphene derivative finds applications in various fields, such as sensors and membranes, where the combination of the hydrophilic GO framework and hydrophobic alkylamine moieties can be tailored for specific interaction requirements and improved performance in diverse environments.

By incorporating 1% (w/w) GO into PCL, the PCL-GO acquires antibacterial and anti-adhesive growth properties, which are time-dependent. We demonstrate these material's features using bacteriophages, bacteria, and eukaryotic cell lines that initially cannot adhere to the printed scaffold. This phenomenon is mediated by a local increase in hydrophobicity due to the GO adsorption of solvent molecules and is fundamental to limit bacteria adhesion during surgical procedures. The phenomenon is strictly dependent also on scaffold geometry, i.e., the possibility of 3D printing in the same scaffold PCL-GO and/or PCL having different heights allows for the control of cell distribution on scaffolds. We also demonstrate that surface wettability increases after repeated contact with biological fluids, and that this consequently increases cell adhesion with time, fundamental for scaffold population and replacement *in vivo*. Due to the GO's ability to absorb infrared (IR) radiation, the scaffold can be sterilized after implantation if biofouling occurs over time. Presently, a limited number of instruments are available for regulating cell adhesion; here, we provide a simple 3D-printing method to facilitate the exploration of bottom-up tissue engineering and its spatial and temporal control.⁴⁰

RESULTS AND DISCUSSION

Characterization of PCL and PCL-GO samples

PCL and PCL-GO (1 wt. %) characterization was performed with several techniques to assess the chemical, optical, morphological, and mechanical properties. The choice of concentration has been made according to literature data. Previous studies have described how a concentration of 1% of reduced GO is well tolerated by cells but, at the same time, does not cause the significant impair of mechanical properties of PCL scaffolds.⁴¹ This concentration is also known to induce differentiation of spindle-like MG-63 cells⁴² and has low cytotoxicity *in vitro*⁴³ and *in vivo* when PCL-G has been used for the production of electric-responsive scaffolds.⁴⁴

In this work, polar solvent-soluble alkylaminated GO has been used to obtain the PCL-GO composite. The FT-IR spectrum of alkylaminated GO [Fig. 1(a), black line] shows the typical band at ≈ 1728 cm⁻¹ due

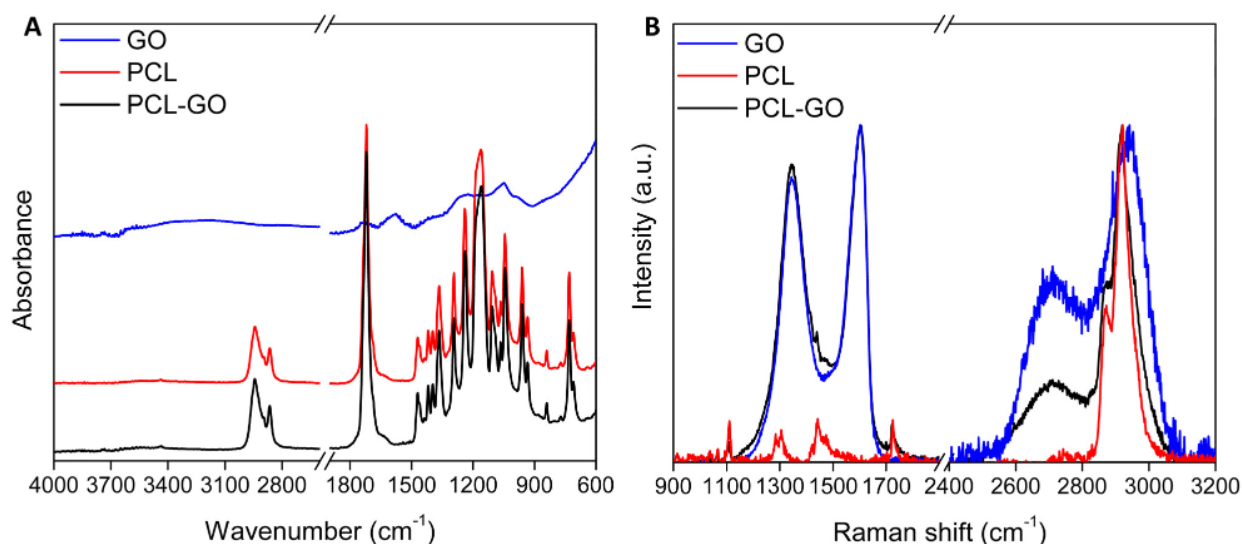


FIG. 1. (a) FT-IR spectra of alkylaminated GO (blue line), PCL (red line), and PCL-GO (black line) and (b) normalized Raman spectra of alkylaminated GO (blue line), PCL (red line), and PCL-GO (black line).

to the stretching vibrations of the carbonyl groups $\nu\text{C}=\text{O}$ of aldehydes, ketones, and carboxyl groups, a further one at $\approx 1580\text{ cm}^{-1}$, tentatively assigned to the $\nu\text{C}=\text{C}$ stretching in the aromatic domains, and a last one at 1225 cm^{-1} , assigned to the C–O stretching mode.^{45–47} Differently, the FT-IR spectrum of the PCL [Fig. 1(a), red line] displays vibrational bands in accordance with the literature.⁴⁸ In particular, the most intense and narrow band localized at $\approx 1720\text{ cm}^{-1}$ and relative to the carbonyl stretching $\nu\text{C}=\text{O}$ almost falls in the same spectral region as that of alkylaminated GO. As expected, the FT-IR spectrum of the PCL-GO composite [Fig. 1(a), blue line] prepared through a simple blending of the two species is indistinguishable from that of PCL one owing to the low amount of GO present in the composite and the absence of chemical derivatization. To gain additional information on the vibrational properties of the materials here presented, a Raman study has been performed. In particular, the Raman spectrum of alkylaminated GO [Fig. 1(b), black line] displays the prominent D band localized at $\approx 1345\text{ cm}^{-1}$ due to the structural defects and G band at $\approx 1600\text{ cm}^{-1}$ related to the planar vibrations mode of the sp^2 hybridized carbon atoms in addition to the less intense second-order 2D and D + G bands centered at ≈ 2706 and $\approx 2942\text{ cm}^{-1}$, respectively. The PCL spectrum [Fig. 1(b), red line] shows the typical weak peaks localized at $\approx 1110\text{ cm}^{-1}$ due to the skeletal vibrations, those within the spectral ranges between 1270 and 1320 cm^{-1} (ωCH_2) and 1405 – 1470 cm^{-1} (δCH_2), at $\approx 1720\text{ cm}^{-1}$ ($\nu\text{C}=\text{O}$), and, finally, the most intense signals relative to the symmetrical ($\nu_s\text{CH}_2$) and asymmetrical ($\nu_{as}\text{CH}_2$) stretching vibrations of the methylene groups localized at 2870 and 2920 cm^{-1} , respectively.^{49–52} The aforementioned signals of the CH_2 groups of PCL, which were also observed in the FT-IR spectra [Figs. 1(a), red and blue lines], are visible in the Raman spectrum of the PCL-GO composite [Fig. 1(b), blue line] whose intensities superimpose to the second-order peaks D + G of GO. In addition, the spectrum of PCL-GO still displays traces of the diagnostic signals of PCL, in particular those localized at ≈ 1110 and

$\approx 1720\text{ cm}^{-1}$, overlapped to the D and G bands characteristic of GO [Fig. 1(b), blue line].^{26,47,53}

The mechanical characterization of scaffolds is reported in Fig. 2. Curves obtained from tensile tests are shown in Fig. 2(a). The addition of GO at a concentration of 1% to PCL results in a $\sim 10\%$ increase in Young's modulus and, consequently, a decrease in the elasticity of PCL-GO compared to PCL [Fig. 2(b)]. This results in a considerable enhancement in the stiffness of PCL-GO compared to PCL. Consequently, the addition of GO leads to a decrease in elasticity, implying that PCL-GO is less capable of returning to its original shape after deformation.

PCL-GO samples also show changes in elongation at break, a critical parameter for understanding a material's ductility and stretchability. Our data indicate a substantial reduction of approximately 23.8% in the elongation at break for PCL-GO in comparison to PCL. This reduction underscores the increased brittleness and reduced ductility of the composite material when GO is introduced [Fig. 2(b)].

We also observed a 15.6% reduction in maximum tensile stress [Fig. 2(c)] and a 12.9% increase in yield stress of PCL-GO [Fig. 2(c)], implying that it can withstand higher stresses before undergoing plastic deformation with respect to PCL.

Our data follow previous findings in the literature; indeed, Kai *et al.* used GO as an enforcing filler of PCL composites⁵⁴ and observed a reduction in the elongation at break and a high reinforcing effect on the material, increasing the yield stress and Young's modulus with increasing volume fraction of GO. Wan and Chen investigated the mechanical behavior of PCL-GO films to exploit their potential bioactivity.⁵⁵ They showed that adding GO at 0.3% (w/w) significantly increased tensile strength, Young's modulus, and energy at break of the PCL membrane. Akhigan *et al.* observed the same shift in the stress–strain curve with their composites of PCL and GO.⁵⁶ In their study, they tested the mechanical changes in PCL scaffolds enriched with GO and with zinc oxide for antibacterial applications. They

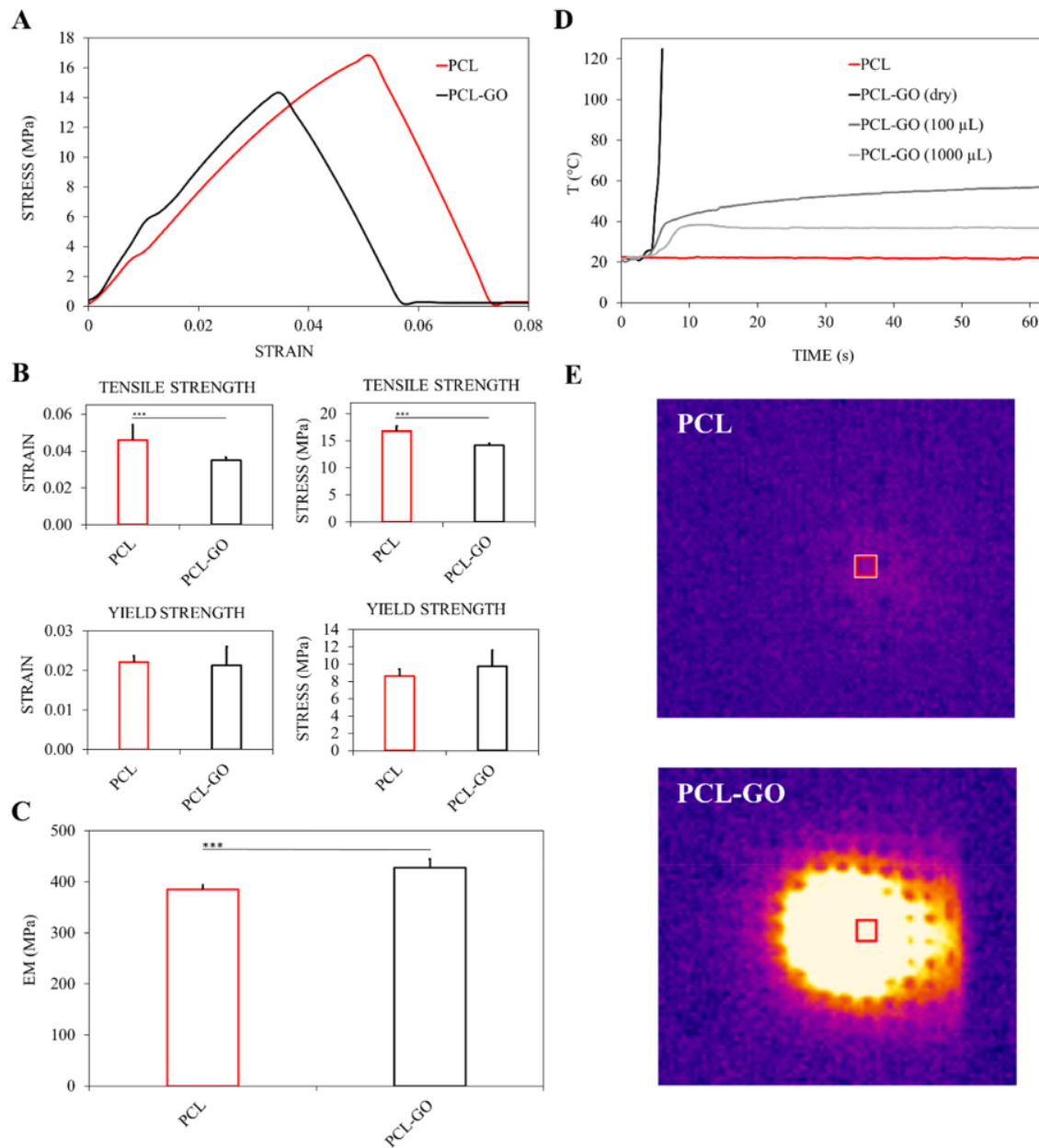


FIG. 2. (a)–(c) Stress–strain curves of PCL and PCL-GO samples and Tensile Strength, Yield Strength, and Young’s Modulus results from mechanical characterization. IR absorption (800 nm) of scaffolds (d) causes an increase in temperature for PCL-GO scaffolds in dry conditions or adding ultrapure water on the surface. A lack of IR absorption has been measured for PCL samples. (e) Representative images of PCL and PCL-GO grids exposed to NIR light obtained with thermal imaging.

reported a significantly increased Young’s modulus along with an improved compressive strength.

Overall, PCL-GO displays increased stiffness, decreased elasticity, reduced ductility, and lower maximum tensile stress compared to PCL.

Figure 2 shows also the response in terms of the temperature reached over time by the samples subjected to infrared laser irradiation monitored by thermal camera. Four types of samples were evaluated:

PCL and PCL-GO in dry conditions, and PCL-GO coated with 100 and 1000 μl of water, respectively.

While PCL samples did not exhibit a significant response to irradiation, the curves for the wet PCL-GO samples reach a plateau at 60.2 °C (PCL-GO 1000 μl) and 37.2 °C (PCL-GO 100 μl). In contrast, the dry PCL-GO sample rapidly heats up, reaching temperatures exceeding 120 °C within the first 10 s with consequent melting. Images

taken with the thermal camera of the samples during irradiation are shown in Fig. 2(e).⁵⁷

Figures 3(a) and 3(b) show representative PCL and PCL-GO 3D-printed grids. Contact angle measurements performed on flat samples are visible in the insets, showing the increase in hydrophobicity in PCL-GO with an increase in the contact angle.

In Figs. 3(c) and 3(d), the SEM images of grid-like structure of the PCL and PCL-GO are reported. Although the distance between the hole centers within the grid remains constant in both PCL and PCL-GO, the area of the holes shows a 49.6% reduction in the latter. The presence of GO and its heat conductive properties ensure a higher temperature uniformity during the 3D printing process, allowing heat to distribute evenly throughout the sample and producing the shown shape. This is confirmed at higher SEM magnification images [Figs. 3(e) and 3(f)], where the surface appears extremely different between PCL and PCL-GO, as confirmed by the detailed surface characterization with AFM [Figs. 3(g) and 3(h)]. Precisely, while PCL is formed by large smooth areas with discontinuities due to an uneven melting of the composite, the surface of PCL-GO has higher uniform roughness.

The roughness was assessed using AFM. The average roughness obtained for PCL on $10 \times 10 \mu\text{m}^2$ area images is $35 \pm 4 \text{ nm}$, whereas it is $100 \pm 20 \text{ nm}$ for PCL-GO. The results obtained confirm the observations made on SEM images and show an increase in the average

roughness for PCL-GO (+286%) compared to PCL. We hypothesize that the different surface morphology is also explained by the GO-modified heat transfer during the 3D printing.

Furthermore, we screened an M13-based phage library to select the most frequent peptides that specifically bind to the scaffolds and to obtain insights about the hydrophobic characteristics of the surface. In Fig. 3(i), we show the X-Gal Agar plates obtained after infection of *E. coli* with phages eluted after three rounds of biopanning. It is visible how the number of colonies is reduced on PCL-GO (10^4 plaques/ml compared to 10^5 plaques/ml for PCL), indicating a smaller amount of phages attached to the surface. Sequence analysis of the peptides enriched during biopanning showed that the aminoacidic stretch of PCL has higher hydrophilicity compared to PCL-GO whose hydrophobicity reduces phage binding [Fig. 3(j)]. The hydrophobicity was calculated as the total average of the amino acids and from the weighted total score for the repeated peptide sequences from the phage recovered. All the indexes confirm a better hydrophilicity for PCL.

Temporal control of PCL-GO scaffolds interaction with eukaryotic cells

To evaluate the biocompatibility, VERO, HEK, C2C12, and RAW cell lines were plated on PCL and PCL-GO scaffolds, and

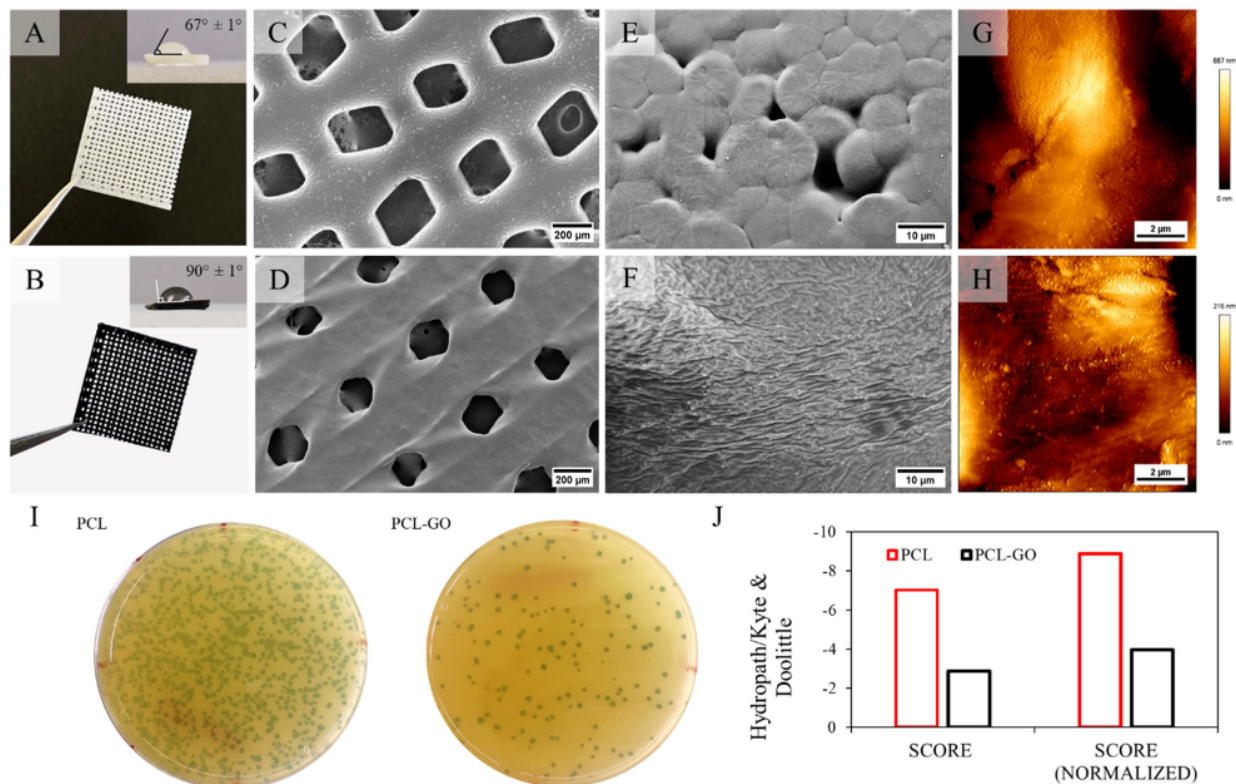


FIG. 3. PCL (a) and PCL-GO (b) grids with respective contact angle measurements. SEM images of PCL (c) and (e) and PCL-GO (d) and (f) grid surface at $200\times$ magnitude (c) and (d) and $5k\times$ magnitude (e) and (f); PCL (g) and PCL-GO (h) AFM characterization of the surface. Phages recovered from each surface have been quantified using blue colonies counting on XGal (i); the average Hydrophath/Kyte & Doolittle values have been calculated considering each sequence (score) or averaging per the number of phages repeated on the surface (normalized score) (j).

cellular viability was evaluated after 72 h by bioluminescence after moving the scaffolds in a new well to quantify the signal from cells directly attached to the surface [Fig. 4(a)]. It was observed that the cellular adhesion on PCL-GO was significantly lower compared to PCL samples. As a control, in Fig. 4(a), the value of cell viability on plastic wells is reported, as expected adhesion on plastic is systematically higher compared to PCL.

PCL is, indeed, relatively hydrophobic, and we have shown how this hydrophobicity increases for PCL-GO samples (Fig. 3). To achieve good cell adhesion, it has been noted that the ideal range for water contact angle values falls between 45 and 70 °C. This is because very high contact angles and low surface energy result in diminished cell-conductive behavior and protein denaturation.⁵⁸ Therefore, we hypothesize that the cell adhesion on PCL-GO is

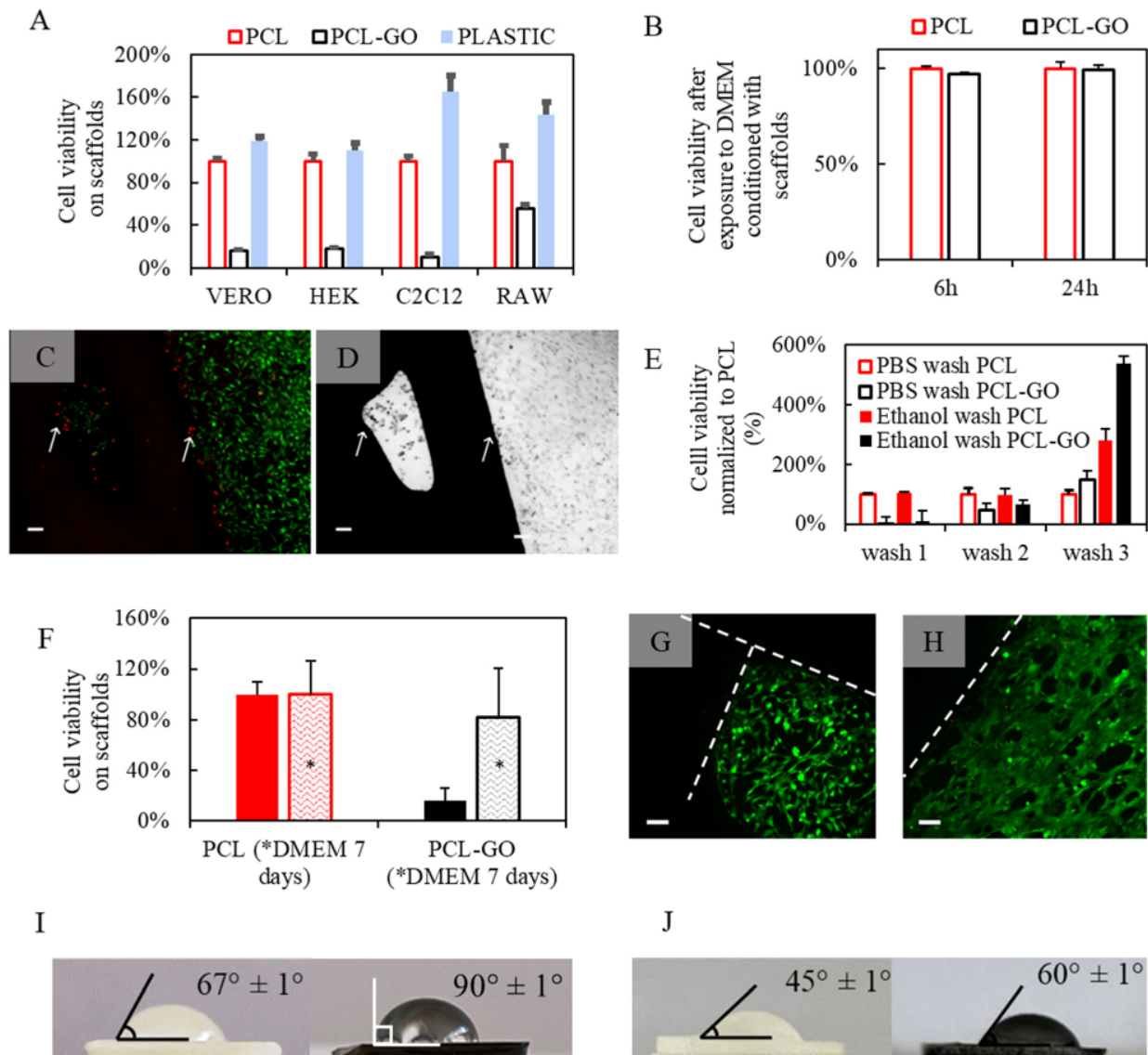


FIG. 4. (a) Viability of different cell lines grown on scaffolds or plastic wells evaluated by luminescence assay. (b) Evaluation of toxicity of DMEM exposed to scaffolds for 7 days and used to treat VERO cells seeded on 96 wells. Toxicity on VERO cells has been evaluated after 6 or 24 h of treatment. (c) Fluorescence imaging of VERO cells surrounding grids of PCL-GO. Cells have been labeled with calcein (green) to evaluate viable cells and propidium iodide (red) to evaluate dead cells. Arrows indicate boundaries between the scaffold and well. The brightfield image of the same sample is shown in (d). (e) Evaluation of VERO cell viability on scaffolds washed with different protocols (PBS or PBS+ethanol). (f) Cell viability on the scaffold after washing with DMEM (indicated with asterisks) or without DMEM washings. (g) and (h) Representative fluorescence images of cells surrounding grids (dashed lines) after DMEM washings, no red dead cells are visible. Scale bar is 100 μ m. Contact angles after one wash in ethanol (i) and after three washes in ethanol (j) show an increased hydrophilicity in the latter case.